CEBAF Program Advisory Committee Six (PAC6) Proposal Cover Sheet

This proposal must be received by close of business on April 5, 1993 at :

CEBAF
User Liaison Office
12000 Jefferson Avenue
Newport News, VA 23606

Proposal Title

High Resolution 1 p shell Hypernuclear spectroscopy

Contact Person

Name : F. Garibaldi
Institution : Physics Laboratory, I.S.S. and INFN Sezione Sanità
Address : Viale Regina Elena 299
Address :
City, State ZIP/Country : Rome, Italy 00161
Phone : + 396 4990 ext 243 **FAX : + 396 446 2872**
E-Mail BITnet : **Internet : Garibaldi @ ISS.INFN.IT**

If this proposal is based on a previously submitted proposal or letter-of-intent, give the number, title and date :

CEBAF Use Only

Receipt Date : 4/5/93 Log Number Assigned : PR 93-015

By : gp

High resolution 1p shell hypernuclear spectroscopy

E.Cisbani, S. Frullani (Co-spokesman), F. Garibaldi (Spokesman), M. Jodice, G.M. Urciuoli
Physics Laboratory, Istituto Superiore di Sanità and INFN Sezione Sanità, Rome, Italy
R. De Leo, R. Perrino
Physics Department, Università di Lecce and INFN Sezione Lecce, Lecce, Italy
M. Sotona
Nuclear Physics Institute , 25068 Rez/Prague, Czech Republic
G.G. Petratos
SLAC, Stanford University, Stanford, CA 94300 *
G.M. Huber, G.J. Lolos
University of Regina, Canada
C.F.Perdrisat and collaborators
(Phys. Dept. College of William and Mary, Williamsburg, Va 23185)
Vina Punjabi and students
(Dept. of Phys. and Chem. Norfolk StateUniversity,Norfolk, Va 23504)
T. Saito and collaborators
(Laboratory of Nuclear Science, Tohoku University)

and

MPS Collaboration

* SLAC is not sponsoring this initiative as an Istitution, given its policy of only supporting research activities at SLAC. The participation of G.G.Petratos is possible because of his fixed term research appointment at SLAC.

ABSTRACT

The goal to study hypernuclear systems with high resolution has been pursued in several Laboratories for many years due to the information on the spin dependence of the effective Λ-N interaction that can be obtained from the energy splitting of hypernuclear spin doublets. At the moment only the electromagnetic production of hypernuclei with electron beam of CEBAF quality together with high resolution spectrometers to detect diffused electrons and produced kaons can afford the possibility to obtain high resolution data (of the order of 100 keV) on hypernuclear spectra.

A high resolution, short orbit spectrometer, as MPS, in combination with one of the HRS with the addition of forward angle capability obtained with a pair of septum magnets could made the CEBAF Hall A the unique facility where this program can become operative.

Physics motivations and a first experimental program on this subject are presented as part of a phisics program that can be done in Hall A if the addition of a third, short path-high resolution magnetic arm is approved.

1. Introduction

Hypernuclear physics is currently an important and exciting part of intermediate energy physics. The Λ-hypernucleus, a nuclear system with the strangeness S=-1, in which the Λ-hyperon replaces one of the nucleons is a long-living baryon system ($\tau \sim 10^{-10}$ s) and provides us with a variety of nuclear phenomena. The hyperon is not excluded from the filled nucleon orbitals by Pauli principle and can penetrate deep inside the nucleus. Weak interactions in the nuclear medium (mesonic $\Lambda \Rightarrow N + \pi$ versus nonmesonic $\Lambda + N \Rightarrow N + N$ decay modes of hypernucleus) can be studied as well as possible modifications of baryon properties (e.g., the magnetic moment of Λ) in the nuclear environment. From low-energy Λp scattering studies [1] we obtained information about the s-state ΛN interaction but the non-central part of ΛN forces is not well established. The better systematics of hypernuclear spectroscopy can help to learn more about the ΛN interaction. Especially useful information on the spin dependence of the effective ΛN interaction can be obtained from the energy splitting of hypernuclear spin doublets.

The theory of low-lying 1p-shell hypernuclear states was restricted for a long time to use the photoemulsion and bubble chamber data on the hypernuclear ground states [2]. The most of the currently available information on hypernuclear excited states come from the strangeness exchange reaction $K^- + n \Rightarrow \pi^- + \Lambda$ with the kaon beam momenta p_K= 400-450 MeV/c or p_K = 700-800 MeV/c. The momentum transferred to the target nucleus is small (q < 100 MeV/c) and the spin-flip transitions for forward pion angles $\Theta_\pi < 10^o$ are negligible in this energy region so that the $\Delta l = \Delta s = 0$ transitions dominate. Due to the strong absorption of the kaon and pion, the reaction takes place on peripheral nucleons. As a result, the substitutional states are predominantly populated. As a rule, the substitutional states lie in the continuum and their interpretation in the framework of the standard shell model calculations is not straightforward.

In the associated production reaction $\pi^+ + n \Rightarrow K^+ + \Lambda$ the momentum transferred is as high as q = 350 MeV/c at p_π = 1.05 GeV/c (the maximum in the elementary cross section). The spin flip part of the elementary amplitude is strong enough to produce an appreciable polarization in the final hypernuclear states [3] but still weak at $\Theta_K < 10^o$, so that the $\Delta l = 1,2$ $\Delta s = 0$ transitions are favoured.It means, that also $p_N \Rightarrow s_\Lambda$ transitions are prefered, but due to the lack of the sufficiently strong spin flip only lower members of the hypernuclear bound states are populated [3].

In addition, the energy resolution of both processes is typically of the order of 2 MeV, the value which is much greater than characteristic spin doublet splitting.

Only the electromagnetic (electro-) production of strangeness on the electron beam of CEBAF quality afford the possibility to obtain the high resolution data on hypernuclear spectra:

(1) the quality of CEBAF beam (high intensity and energy resolution) make possible, at least in principle, to identify the bound hypernuclear levels with a resolution at the level of ~100 keV,

(2) due to the strong spin flip contribution, the both members of spin doublet may be populated,

(3) contrast to (K^-,π^-) and (π^+,K^+), electromagnetic production of $K^+\Lambda$ pair goes on the proton making possible to study the hypernuclei non available otherwise ($^7He_\Lambda$, $^9Li_\Lambda$,....).

A typical example (^{12}C target) of the spectroscopic information which can be obtained from (K^-,π^-), (π^+,K^+) and $(e,e'K^+)$ reactions is shown in Fig. 1.

2. Shell model description of hypernuclear spectra

The many particle shell model is used, by analogy with spectroscopy of light nuclei, to describe the 1p-shell hypernuclear spectra quantitatively in terms of the $|s^4p^{A-5} * s_\Lambda; JT\rangle$ configurations. As was shown many times [4-5], the available hypernuclear data from (K^-,π^-), $(K^-,\pi^-\gamma)$ and (π^+,K^+) may be adequately described by weak coupling model. In this model the Λ-hyperon in 0s shell is coupled to certain nuclear state of the parent nucleus with spin and parity J_{A-1} ,π creating doublet of states $J = J_{A-1} \pm 1/2$. Hypernuclear states belonging to different doublets mix only weakly, as a rule, and doublet energy splitting is therefore determined by spin dependent part of the effective ΛN interaction alone.

The two-body lambda - nucleon effective interaction may be expressed in the form [4]

$$V_{\Lambda N}(r) = V(r) + V_\sigma(r)s_\Lambda.s_N + V_\Lambda(r)s_\Lambda.l_{N\Lambda} + V_N(r)s_N.l_{N\Lambda} + V_T(r)S_{12} \qquad (1)$$

where $l_{N\Lambda}$ is the relative $N\Lambda$ orbital momentun and S_{12} - tensor operator. Then, the interaction can be expressed in terms of five radial integrals, one associated with each term in (1). These parameters, denoted by V (central interaction), Δ (spin-spin), S_Λ, S_N (lambda and nucleon spinorbit) and T (tensor) are supposed to be constant throughout the 1p-shell.

The doublet splittings are determined mainly by Δ, S_Λ and T, while S_N affects the spacing between different doublets. The averaged central interaction has no effect on spectra, but determines (together with three-body ΛNN forces, if present) the binding energies B_Λ of hypernuclear ground states.

Previous attempts to investigate the spin dependence of the ΛN effective interaction in light hypernuclei were limited by a lack of data. In the first serious phenomenological analysis [4] 12 bound state energies together with the constraints imposed by a knowledge of three ground states spins were used as a data input to the fit. The optimum version (called *canonical* in [5]) of the parameters (in MeV)

$$V = 1.23, \quad \Delta = 0.15, \quad S_\Lambda = 0.57, \quad S_N = -0.21, \quad T = 0 \qquad (C)$$

predicts rather large doublet splittings (~ 1 MeV - see Fig's 2-5, model C).

However, the later experiments [6-7] where γ-lines from $^7Li_\Lambda$ and $^9Be_\Lambda$ in $(K^-,\pi^-\gamma)$ reaction were measured, have not confirmed the position of $5/2^+$ level in $^7Li_\Lambda$ (predicted by canonical set at 1.35 MeV; Eexper = 2.034 ± 0.023 MeV) and the strong splitting of $(3/2^+,5/2^+)$ first excited doublet in $^9Be_\Lambda$ ($\delta = 3.66(5/2^+) - 2.09(3/2^+) = 1.57$ MeV; in the experiment only one γ-line was detected with E = 3.08 MeV).

To overcome the difficulties, Millener, Gal, Dover and Dalitz [8] proposed an alternative set of parameters (*standard* - S):

$$\Delta = 0.50, \quad S_\Lambda = -0.04, \quad S_N = -0.08, \quad T = 0.04 \qquad (S)$$

The predicted doublet splittings, compared with the canonical set (C), are much smaller (see Fig's. 2-5, model S). Guided by the predictions of the doublet splittings in the 1p-shell hypernuclei, the BNL experimental group made an attempt to detect the γ-transitions $2^- \Longrightarrow 1^-$ (gr. st.) with $E_\gamma = 170$ keV in $^{10}B_\Lambda$ and $1^- \Longrightarrow 0^-$(gr.st.) with $E_\gamma = 80$ keV in $^{16}O_\Lambda$ [9-10]. No such hypernuclear γs were observed between 80 to 510 keV.

As a solution of the puzzle, another set of parameters was proposed by Majling, Fetisov, Zofka and Eramzhyan (*FMZE*) [11]:

$$\Delta = 0.3, \quad S_\Lambda = -0.02, \quad S_N = \begin{matrix} \text{-0.35 for } ^7Li_\Lambda \\ \text{-0.1 for A>7} \end{matrix}, \quad T = 0.02 \qquad \text{(FMZE)}$$

The puzzle is solved on the price that:

1) the set (FMZE) is valid only for 1p-shell hypernuclei and the position of $J=1^+$ levels in $^4H_\Lambda$ and $^4He_\Lambda$ cannot be explained by it.
2) the parameter set is partially A-dependent: $S_N = -0.35$ for $^7Li_\Lambda$ and $S_N = -0.1$ otherwise. The $^7Li_\Lambda$ anomaly is motivated in [11] by the fact that the shell model is not adequate for this cluster hypernucleus $^7Li_\Lambda = \{^4He + d + \Lambda\}$. The obtained hypernuclear energy spectra are again shown in Fig's. 2 - 5 and denoted as FMZE.

The situation, from the experimental as well as from the theoretical point of view, has to be clarified. Only a few 1p-shell hypernuclear levels and γ transitions between them have been observed experimentally (see e.g. review of data in [12]). In addition, only the γ-lines from $^7Li_\Lambda$ ($5/2^+ \Rightarrow 3/2^+$, E=2.03 MeV) and $^9Be_\Lambda$ ($(5/2^+,3/2^+) \Rightarrow 1/2^+$; E=3.08 MeV), corresponding to the transitions between different spin doublets are well identified. The γ-ray information on the spin doublet splittings is either not well confirmed ($^7Li_\Lambda$ ($3/2^+ \Rightarrow 1/2^+$;

E=0.44 MeV), $^{9}Li_{\Lambda}$ ($5/2^{+}$ => $3/2^{+}$; E=0.31 MeV), or it has not a character of the positive evidence (missing γ-lines from ground state doublets in $^{10}B_{\Lambda}$ and $^{16}O_{\Lambda}$). In the near future, the only possibility of essential progress in this direction is given by the high resolution (~100 keV) hypernuclear spectroscopy with electron beam, and CEBAF is the only accelerator in the world in which this program can be accomplished, or with other facilities still under considerations (Pilac).

3. Electroproduction of hypernuclei

Our estimates of the electroproduction cross-sections on ^{7}Li, ^{9}Be, ^{12}C and ^{16}O targets are based on the following assumptions (see also [13]):

1) DWIA; kaon distortion is calculated in eikonal approximation (p_K ~ 1 GeV/c, relatively weak absorption by nuclei)
2) the electroproduction models based on effective Lagrangian theory with strong coupling constants fitted to available photoproduction data. The dependence of predicted strength function for ^{12}C target (E_e = 3 GeV, $E_{e'}$ = 1.5 GeV, $\Theta_e = 7^{o}$ and $\Theta_K = \Theta_\gamma = 7^{o}$) on the models of elementary process $e + p \Rightarrow e' + K^{+} + \Lambda$ is illustrated in Fig. 6. The strength functions are given for C2 model [14] (largest cross-section), AB2 model [15] (smallest one) and TH1 model [16] (an intermediate case). The model dependence for strongly excited states is not too strong, of the order of ±15%, the value which is quite comparable with other uncertainties in the calculations of this type.
3) shell model nuclear and hypernuclear wave functions are calculated with effective NN interaction of Utrecht group [17] including the $1\hbar\omega$ opposite parity states. As an effective ΛN interaction we use the one derived in [18] from Nijmegen soft core hyperon -nucleon interaction. It means that our ΛN effective interaction contain no free parameters, but Fermi momentum (nuclear density).If the calculated energy of the underlying nuclear level of parent nucleus (^{6}He, ^{8}Li, ^{11}B and ^{15}N) does not agree with it experimental value, it is moved "by hands" to it experimental position. Corresponding hypernuclear energy spectra are denoted YNG in Fig's. 2-5. Our predicted doublet splittings are sometimes in sharp disagreement with other models. Nevertheless, we believe that it will not influence [11] too much the hypernuclear wave functions and estimated cross sections.

Momentum transfer to the hypernucleus in the electroproduction is rather large (q ~ 400 MeV/c for light nuclei) and decreases steadily with increasing energy of virtual photon $E_\gamma = E_e - E_{e'}$. The photoproduction cross section, with K at forward angle, is almost constant for E_γ =1.2-1.5 GeV. It suggest that E_γ ~ 1.5 GeV should be an optimum choice. The dependence of the production cross section for $J = 2^{-}$, E = 0.03 MeV and $J=3^{+}$, E=10.63 MeV states of $^{12}B_{\Lambda}$ on virtual photon energy is shown in Fig. 7. Energy of scattered

electrons $E_{e'} = 0.3$ GeV is kept constant, electron scattering angle $\Theta_e = 7^o$ and kaon scattering angle $\Theta_K = \Theta_\gamma$ (in the virtual photon direction). The cross section for bound $J = 2^-$ state increases steadily with increasing photon energy, the same value for the (p^{-1}, p_Λ) $J = 3^+$ state remains almost constant in the energy range $E_\gamma = 1.1 - 2.0$ GeV. To obtain maximum cross-section we have to keep the electron scattering angle as small as possible (large virtual photon flux) - Fig. 8 - and kaon scattering angle close to the virtual photon direction $\Theta_K = \Theta_\gamma$ - Fig. 9. In both cases $E_e = 3$ GeV, $E_{e'} = 1.5$ GeV and the cross-section for ^{12}C (e,e'K+) $^{12}B_\Lambda$(J=2⁻; E=0.03 MeV) and (J=3⁺, E=10.63 MeV) is shown. For the Θ_e dependence (Fig. 8) $\Theta_K = \Theta_\gamma$ and in Fig. 9 $\Theta_e = 7^o$. We can see that to keep $\Theta_e \leq 10^o$ and $|\Theta_K - \Theta_\gamma| \leq 10^o$ is a crucial requirement. The value of the optimum kaon scattering angle ($\Theta_K = \Theta_\gamma$) for fixed photon energy $E_\gamma = E_e - E_{e'}$ and fixed electron scattering angle Θ_e as a function of beam energy E_e is visualized in Fig. 10. It is seen that from the point of view of experimental geometry the higher beam energies are preferable (large Θ_γ), but on the cost that additional K^+ production channels (higher hyperon resonances etc) will open.

At last, Fig's. 11-14 show the calculated strength functions at $E_e = 3$ GeV, $E_{e'} = 1.5$ GeV, $\Theta_e = 7^o$ and $\Theta_K = \Theta_\gamma = 6.9^o$ for ^7Li, ^9Be, ^{12}C and ^{16}O targets. In all cases the C1 [14] electroproduction model is used and energy resolution $\Gamma = 0.1$ MeV is supposed for bound hypernuclear levels. For unbound levels (above the strong decay threshold) the uniform escape width $\Gamma = 2$ MeV is assumed.

In $^7He_\Lambda$ the predicted production rates for $3/2^+$ and $5/2^+$ members of the first excited doublet (built on $J=2^+$, E = 1.8 MeV first excited state of ^6He core nucleus) are comparable but, unfortunately, much smaller (~ 0.1 nb/sr**2/GeV) than the cross-section to the $^7He_\Lambda$ ground state.

In $^9Li_\Lambda$ the low-spin members of all three spin doublets (ground state and the doublets built on $J=1^+$ E=0.98 MeV and $J=3^+$, E=2.25 MeV excited states of ^8Li) are rather weakly populated in comparison with high-spin ones. However, the valuable information on the relative positions of different doublets (and consequently on nucleon spinorbit parameter S_N of ΛN effective interaction) probably may be obtained in this way.

The similar situation (only one member of each doublet is strongly populated) is examined for $^{12}B_\Lambda$ hypernucleus. In addition, the ground state doublet is nearly degenerated in all models and unresolvable with energy resolution ~100 keV.

The $^{12}B_\Lambda$ hypernucleus is extremely bound one, $E_{thr} = 11.37$ MeV. It is supposed, therefore, that some of the positive parity states ($J= 0^+, 1^+, 2^+, 3^+$) at Ex ~ 10-11 MeV with (p^{-1},p_Λ) structure may be particle stable. The $|p_{3/2}(\Lambda) * {}^{11}C(J=3/2^-,gr.st.); J=0^+\rangle$state strongly populated in (K^-,π^-) recoil reaction is predicted at $E_x \approx 10.6$ MeV in mirror $^{12}C_\Lambda$ hypernucleus [19], but this state is not populated in (e,e'K⁺). Two $J = 2^+$ states with a structurel $|p_j(\Lambda) * {}^{11}C(J=3/2^-,gr.st.);J=2^+\rangle$ were also found in [19], one at approximately the

same position as $J=0^+$ one and another one about 0.8 MeV lower. These states were seen not only in emulsion experiments [19] but also in (π^+,K^+) reaction on ^{12}C target. Due to the strong spin-flip in $(e,e'K^+)$ reaction, also $J=1^+$ and especially $J=3^+$ members of this multiplet may be populated (see Fig. 13). Taking into account the large binding energy of the mirror $^{12}B_\Lambda$ hypernucleus, at least some of these states may be particle stable here.

The situation seems to be much better in $^{16}N_\Lambda$ hypernucleus. The both members of ground state as well as excited state doublet are populated with sufficient strengths. The careful investigation of ground state doublet can confirm or question commonly accepted assumption of nearly degenerate $^{16}N_\Lambda$ ground state doublet [8,11]. The precise measurement of the splitting of the first excited $(1^-,2^-)$ doublet at $E_x \sim 6.5$-7 MeV would allow for the first time to extract directly from experimental data extremely valuable information on the tensor component T of the ΛN interaction. It is known well [8] that the tensor force T dominates the doublet splittings in the upper half of 1p-shell.

In high resolution $(e,e'K^+)$ it will be probably also possible to obtain an interesting spectroscopic information from the positions and escape widths of some 1 hω hypernuclear states $((p^{-1},p_\Lambda)$ and (s^{-1},s_Λ) in some cases). This states are particle unstable as a rule (with already mentioned exception of $^{12}B_\Lambda$), but the estimated escape widths of many of them are rather small, few tens keV to 1 MeV [12]. A typical example is a $J = (3/2^-,5/2^-)$ doublet at $Ex \approx 15$ - 17 MeV in $^7He_\Lambda$ with estimated widths $\Gamma \approx 2$ MeV [20].The lower member $J = 3/2^-$ of the doublet is well seen in (K^-,π^-) reaction on ^7Li [20]. In $(e,e'K^+)$ reaction the both members of the doublet should be populated - Fig. 11.

It was argued in [12] that the widths of some particle unstable states in the second half of the 1p shell may be very small. It is predicted e.g. that some $J = 2^+$ states in $^{16}O_\Lambda$ ($^{16}N_\Lambda$) at excitation energy approximately 10-15 MeV will be as small as $\Gamma \approx 15$-40 keV, instead of the fact that $E_{thr} = 6.9$ MeV only for $^{16}O_\Lambda$. The states of this type in mirror $^{16}N_\Lambda$ hypernucleus are also distinguishable in $(e,e'K^+)$ - Fig. 15. Careful investigation of the position and especially of width of these states may serve as a valuable check of hypernuclear wave functions and decay mechanism.

4. Kinematical conditions and counting rates

The kinematical and experimental conditions for (e,e'k) experiments on ^7Li, ^9Be, ^{12}C and ^{16}O targets are reported in table I. They are the same for all the measurements performed on the different targets.

TABLE I
Kinematical conditions

Electron beam energy	Ein	= 3 GeV
Scattered electron energy	Eout	= 1.5 GeV
Scattered electron angle	Θ_e	= 7 deg
electron momentum acceptance	$\Delta E/E$	= +/- 5 %
electron solid angle	$\Delta\Omega$	= 2 msr
kaon momentum	Pk	= 1.209 GeV/c for ^{7}Li and ^{12}C 1.220 GeV/c for ^{9}Be and ^{16}O
kaon momentum acceptance	$\Delta P/P$	= +/- 7.5 %
kaon angle = virtual photon angle	Θ_k	= 6.9 deg
kaon solid angle	$\Delta\Omega$	= 10 msr
Incident flux	N_e	= 6.24 10^{14} (I = 100 μA)
Target thickness	t	= 100 mgr/cm^2
kaon survival probability	f	= 40 %

The luminosity, obtained with constant beam current of 100 μA and target thickness of 100 mg/cm^2 ranges from 5.4 10^{36} cm^{-2}sec^{-1} in the case of ^{7}Li to 2.3 10^{36} cm^{-2}sec^{-1} for ^{16}O.

For the electron arm, the characteristics of the HRS spectrometer of the Hall A experimental equipment, working at forward angles (less than 13°), are considered. As regards the kaon arm, typical characteristics of the Multi Purpose Spectrometer (MPS) design [21], are taken into account. Among its features, such a device is designed to be short enough to contain kaon trajectories, from the target up to the focal plane detection system, in relatively short paths of about 12 meters, giving a rather high kaon survival probability for kaon momenta greater than 1 GeV (about 40 % at 1.2 GeV). For both spectometers the forward scattering angles capability is considered with the use of two septum magnets [21].

MPS has high momentum resolution: $\delta p/p \sim 10^{-4}$. This is a very important requirement for the physics of hypernuclei, for which a total energy resolution at the level of (few) hundreds KeV is needed in order to separate and locate in the energy spectrum, different hypernuclear levels. With the properties of the CEBAF electron beam and the considered spectrometers, the level of 100 KeV in energy resolution could be achieved in (e,e'k) experiments with thin targets . In our case the targets proposed have thickness of 100 mg/cm^2. In this case they are not thin enough to reach the required resolution due to the spread in energy caused by the energy loss in the target which depends on the interaction point. To obtain a better resolution, it is possible to split the target in several thinner targets (see fig. 16) with the optical properties

of the spectrometer allowing the identification of the source target point and hence the eventual correction for the known energy loss in the crossed targets other than that from where the kaon is knocked-out.

An example of the gain in resolution with this method can be seen in figures 17a and 17b. Fig. 17a shows a Monte Carlo simulation of the momentum spread distribution for a kaon produced with a momentum of 1.5 GeV/c at the vertex of interaction in a ^{12}C target of 100mg/cm^2. Fig. 17b shows the spread when the kaon is produced in the third layer out of five identical subsequent layers with a thickness of 20 mg/cm^2 with the inclusion of the straggling caused by the two subsequent layers. While in the first case a spread of about 150 KeV/c is obtained, giving a big contribution to the resolution, in the second case one has a spread of about 40 KeV/c that allows to reach the required resolution. The shift in momentum is due to the energy loss in the fourth and fifth target and it is a calculable quantity.

Moreover a splitted target allows to reduce the accidental coincidence rate if the origin from the same target is imposed to the electron and kaon detected in coincidence.

In this scheme the contribution to the resolution of the primary electron beam is the most important and to achieve a 100 keV resolution the primary beam must be dispersed on the target and the double dispersion matching technique has to be used.

The single events and accidental coincidences counting rates result to be quite constant for all the investigated nuclei and the numbers reported in table II represent upper limits in our conditions.

TABLE II

Single and accidental rates

(e,e') single rate	1.1 10^5 (sec^{-1})
(e,k) single rate	4.7 10^3 (sec^{-1})
(e,p) single rate	4. 10^7 (sec^{-1})
(e,π) single rate	7. 10^6 (sec^{-1})
accidental (e,e'k)	4.1 (sec^{-1}) (full acceptance)
accidental (e,e'k)	1.8 (hour^{-1}) per 200 KeV bin
accidental (e,e'k)	0.35 (hour^{-1}) per 200 KeV bin for splitted target (5x20mg/cm^2)

The single electron arm counting rates are computed with the QFS code of Lightbody and O'Connel [22] with the added contribution of the elastic radiative tail which gives electron elastically scattered into the spectrometer after having loss the right energy through bremsstrahlung emission of real photons in the target. This contribution has been estimated

by means of the approximated formula C.11 of ref.[23].

The proton and pion background has been estimated with the EPC code of Lightbody and O'Connel [22]. This directive background is the biggest problem when MPS operates in small forward angle mode. This implies an accurate design of the detector package and a careful choice of the electronics already commercially available. From the numbers reported one sees that the detector system must have a rejection factor of 10^4 and 2.10^3 for protons and pions against kaon, respectively.

The kaon rate is estimated following the procedures suggested in ref. [24]. The accidental rates are calculated considering a time coincidence of 1 ns and a duty cicle of 100% and are reported in the table for the full acceptance (in sec^{-1}) as well as for a 200 KeV bin (in $hour^{-1}$).

Cross sections, calculated as specified in the previous chapter, and expected counting rates for different hypernuclear levels populated in $^7Li(e,e'K)^7He_\Lambda$, $^9Be(e,e'k)^9Li_\Lambda$, $^{12}C(e,e'k)^{12}B_\Lambda$ and $^{16}O(e,e'k)^{16}N_\Lambda$ experiments are reported in tables IIIa-d.

TABLE IIIa $^7Li(e,e'K)^7He_\Lambda$ cross sections and counting rates

Level	(e,e'K) (nb/GeV/sr^2)	Rate (e,e'k) (hour^{-1})
ground state J = 1/2$^+$	0.37	8.4
E=1.59 MeV J = 5/2$^+$	0.084	2.0
E=1.94 MeV J = 3/2$^+$	0.064	1.5

TABLE IIIb $^9Be(e,e'k)^9Li_\Lambda$ cross sections and counting rates

Level	(e,e'K) (nb/GeV/sr^2)	Rate (e,e'k) (hour^{-1})
E=0.7 MeV J = 5/2$^+$	0.45	8.1
E=1.71 MeV J = 3/2$^+$	0.134	2.4
E=2.79 MeV J = 7/2$^+$	0.143	2.6

TABLE IIIc $^{12}C(e,e'k)^{12}B_\Lambda$ cross sections and counting rates

Level	(e,e'K) (nb/GeV/sr^2)	Rate (e,e'k) (hour^{-1})
ground state J = 1$^-$	0.33	4.4
E=0.03 MeV J = 2$^-$	2.02	27.3
E=2.54 MeV J = 1$^-$	0.83	11.2
E=5.46 MeV J = 2$^-$	0.27	3.6
E=10.03 MeV J = 3$^+$	0.35	4.7
E=10.63 MeV J = 3$^+$	1.59	21.5
E=11.22 MeV J = 2$^+$	0.31	4.2

TABLE IIId $^{16}O(e,e'k)^{16}N_\Lambda$ cross sections and counting rates

Level	(e,e'K) (nb/GeV/sr^2)	Rate (e,e'k) (hour^{-1})
ground state J = 1$^-$	1.05	10.6
E=0.44 MeV J = 0$^-$	0.16	1.6
E=6.89 MeV J = 1$^-$	0.77	7.8
E=7.03 MeV J = 2$^-$	2.13	21.6
E=9.18 MeV J = 2$^+$	0.11	1.1
E=10.81 MeV J = 2$^+$	1.10	11.2

5. Beam time requests

According to the (e,e'k) coincidence event rates reported in Tables III, the less populated levels in which we are interested give a contribution of about 2 counts/hour to the total counting. The accidental counting rate is almost a factor ten less, then it does not influence the statistical accuracy in a substantial way. With 200 hours of beam time per nucleus a statistical accuracy of about 5% for these levels is obtained, while for the more populated levels an accuracy better than 2% is achieved. Adding 25% of beam time to take into account calibration and contingency, we think that with 1000 hours of beam time a first complete study of high resolution hypernuclear spectroscopy in p shell nuclei can be accomplished.

References

[1] G. Alexander et al.:Phys. Rev. 173 (1968) 1452

[2] J. Pniewski et al.: Nucl. Phys. A443 (1985) 685

[3] H. Bando, T. Motoba, M. Sotona, and J. Zofka: Phys. Rev. C39 (1989) 587

[4] A. Gal, J. M. Soper, and R. H. Dalitz: Ann. Phys. (N.Y.) 63 (1971) 53; 72 (1972) 445; 113 (1978) 79

[5] R. H. Dalitz and A. Gal: Ann. Phys. (N.Y.) 116 (1978) 167

[6] M. Bedjidian et al.: Phys. Lett. 83B (1979) 252

[7] M. May et al.: Phys. Rev. Lett. 51 (1983) 2085

[8] D. J. Millener, A. Gal, C. B. Dover, and R. H. Dalitz: Phys. Rev. C31 (1985) 499

[9] R. E. Chrien: Czech. J. Phys. B39 (1989) 914; Nuovo Cim. 102A (1989) 727

[10] R. E. Chrien et al.: Phys. Rev. C41 (1990) 1082

[11] V. N. Fetisov, L. Majling, J. Zofka, and R. A. Eramzhyan: Z. Phys. A339 (1991) 399
preprint 102, Lebedev Phys. Inst., Moscow 1990

[12] L. Majling, R. A. Eramzhyan, and V. N. Fetisov: Czech. J. Phys. 42 (1992) 1197

[13] J. Adam, J. Mares, O. Richter, M. Sotona, and S. Frullani: Czech. J. Phys. 42 (1992) 1167

[14] R. A. Williams, Ch.-R. Ji, and S. R. Cotanch: Phys. Rev. C43 (1991) 452

[15] R. A. Adelseck, C. Benhold, and L. E. Wright: Phys. Rev. C32 (1985) 1681

[16] H. Thom: Phys. Rev. 151 (1966) 1322

[17] A. G. M. van Hees and P. W. M. Glaudemans: Z. Phys. A314 (1983) 323

[18] Y. Yamamoto and H. Bando: Prog. Theor. Phys. 73 (1985) 905

[19] R.H. Dalitz, D.H. Davis, D.N. Tovee: Nucl. Phys. A450 (1986) 311c

[20] O. Richter, M. Sotona, J. Zofka: Phys. Rev. C43 (1991) 2753

[21] S.Frullani, F.Garibaldi, F.Ghio, M.Jodice, G.M.Urciuoli, R.De Leo, Multi Purpose Spectrometer, I.N.F.N. - I.S.S. 90/5, July 1990

[22] J.W.Lightbody Jr., J.S.O'Connel, Comp.in Physics, May/June 1988, p.57

[23] L.W.Mo and Y.S.Tsai, Rev. Mod. Phys. 41(1969)205

[24] C.E. Hyde-Wright, W.Bertozzi, J.M.Finn Proc. of the 1985 CEBAF Workshop

Figure captions

Fig. 1. Strength functions for (K^-,π^-), (π^+,K^+) and $(e,e'K^+)$ reactions on ^{12}C target

Fig. 2. Predicted energy spectra of $^{7}He_{\Lambda}$

Fig. 3. Predicted energy spectra of $^{9}Li_{\Lambda}$

Fig. 4. Predicted energy spectra of $^{12}B_{\Lambda}$

Fig. 5. Predicted energy spectra of $^{16}N_{\Lambda}$

Fig. 6. Strength function for $^{12}C(e,e'K^+)^{12}B_{\Lambda}$ reaction and different models: AB2 [15] - solid line, C2 [14] - dots, and TH1 [16] - dashed line. E_e = 3 GeV, $E_{e'}$ = 1.5 GeV, $\Theta_e = 7^o$ and $\Theta_K = \Theta_\gamma = 7^o$.

Fig. 7. The dependence of the $^{12}C(e,e'K^+)^{12}B_{\Lambda}$ cross section on the energy E_γ of virtual photon for $J=2^-$, E=0.03 MeV (solid line) and $J=3^+$, E=10.66 MeV (dashed line) states of $^{12}B_{\Lambda}$. $E_{e'}$ = 0.3 GeV, $\Theta_e = 7^o$ and $\Theta_K = \Theta_\gamma$.

Fig. 8. The dependence of the $^{12}C(e,e'K^+)^{12}B_{\Lambda}$ cross section on the electron scattering angle Θ_e for $J=2^-$, E=0.03 MeV (solid curve) and $J=3^+$, E=10.66 MeV (dots) states of $^{12}B_{\Lambda}$. E_e = 3 GeV, $E_{e'}$ = 1.5 GeV, $\Theta_K = \Theta_\gamma$.

Fig. 9. The same as in Fig. 8, but as a function of the kaon scattering angle at $\Theta_e = 7^o$.

Fig. 10. Virtual photon scattering angle Θ_γ for fixed $E_\gamma = E_e - E_{e'}$ and $\Theta_e = 7^o$ as a function of beam energy E_e.

Fig. 11. Predicted strength function for $^{7}Li(e,e'K^+)^{7}He_{\Lambda}$ reaction with C2 [14] elementary amplitude. E_e = 3GeV, $E_{e'}$ = 1.5 GeV, $\Theta_e = 7^o$ and $\Theta K = \Theta\gamma = 6.9^o$.

Fig. 12. The same as in Fig. 11 for $^{9}Be(e,e'K^+)^{9}Li_{\Lambda}$

Fig. 13. The same as in Fig. 11 for $^{12}C(e,e'K^+)^{12}B_{\Lambda}$

Fig. 14. The same as in Fig. 11 for $^{16}O(e,e'K^+)^{16}N_{\Lambda}$

Fig. 15. Entire and splitted target arrangements

Fig. 16.a),b) Monte Carlo simulation of the measured momentum spread distribution for a kaon of 1.5 GeV/c at the interaction point: a) in the case of entire target of 100mg/cm2; b) case of splitted target (5x20mg/cm2)

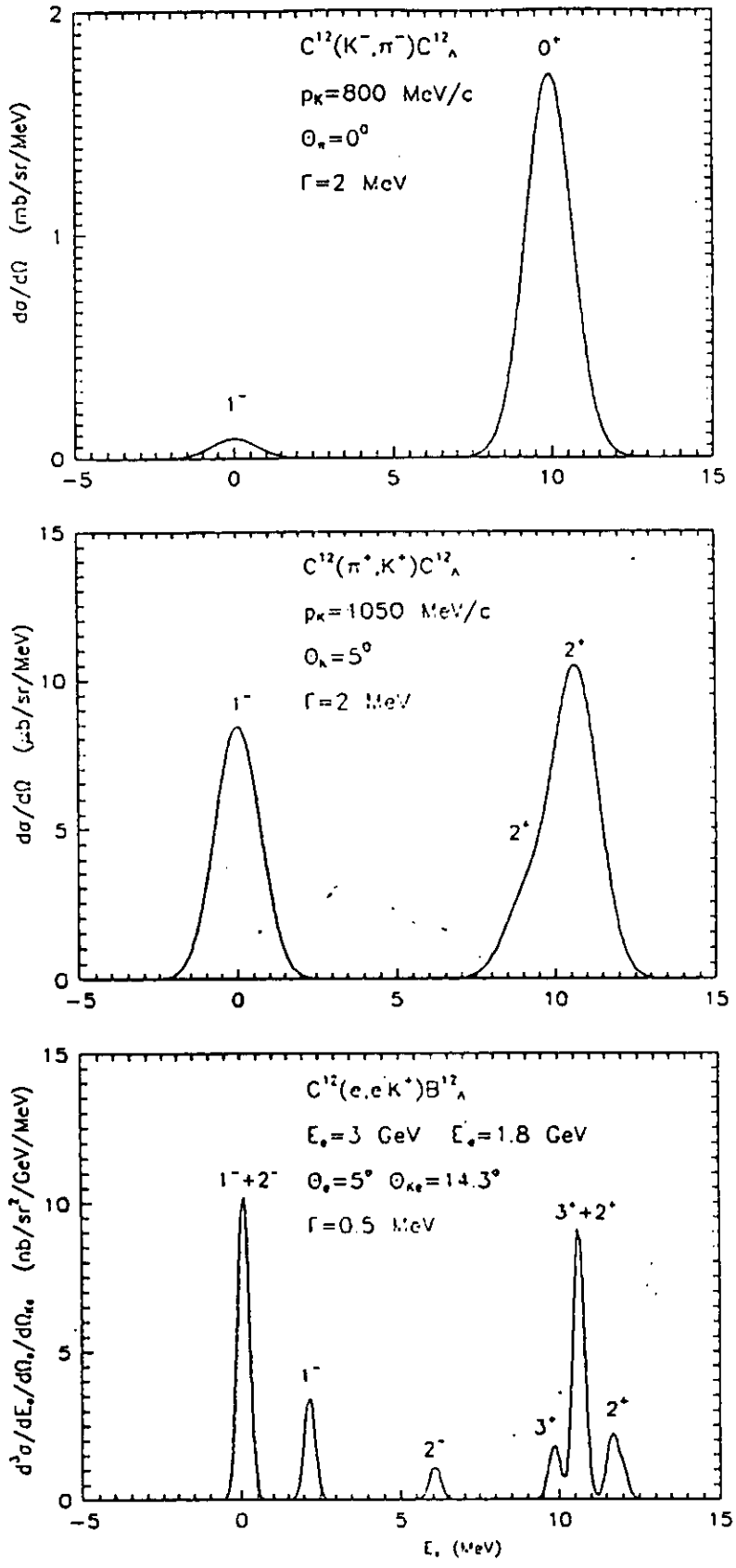
$C^{12}(K^-,\pi^-)C^{12}_\Lambda$
p_K=800 MeV/c
Θ_π=0°
Γ=2 MeV
1⁻
0⁺
dσ/dΩ (mb/sr/MeV)
$C^{12}(\pi^+,K^+)C^{12}_\Lambda$
p_K=1050 MeV/c
Θ_K=5°
Γ=2 MeV
1⁻
2⁺
2⁺
dσ/dΩ (μb/sr/MeV)
$C^{12}(e,e'K^+)B^{12}_\Lambda$
E_e=3 GeV E'_e=1.8 GeV
Θ_e=5° Θ_{Ke}=14.3°
Γ=0.5 MeV
1⁻+2⁻
1⁻
2⁻
3⁺
3⁺+2⁺
2⁺
$d^3\sigma/dE_e/d\Omega_e/d\Omega_{Ke}$ (nb/sr²/GeV/MeV)
E_x (MeV)

Fig. 1

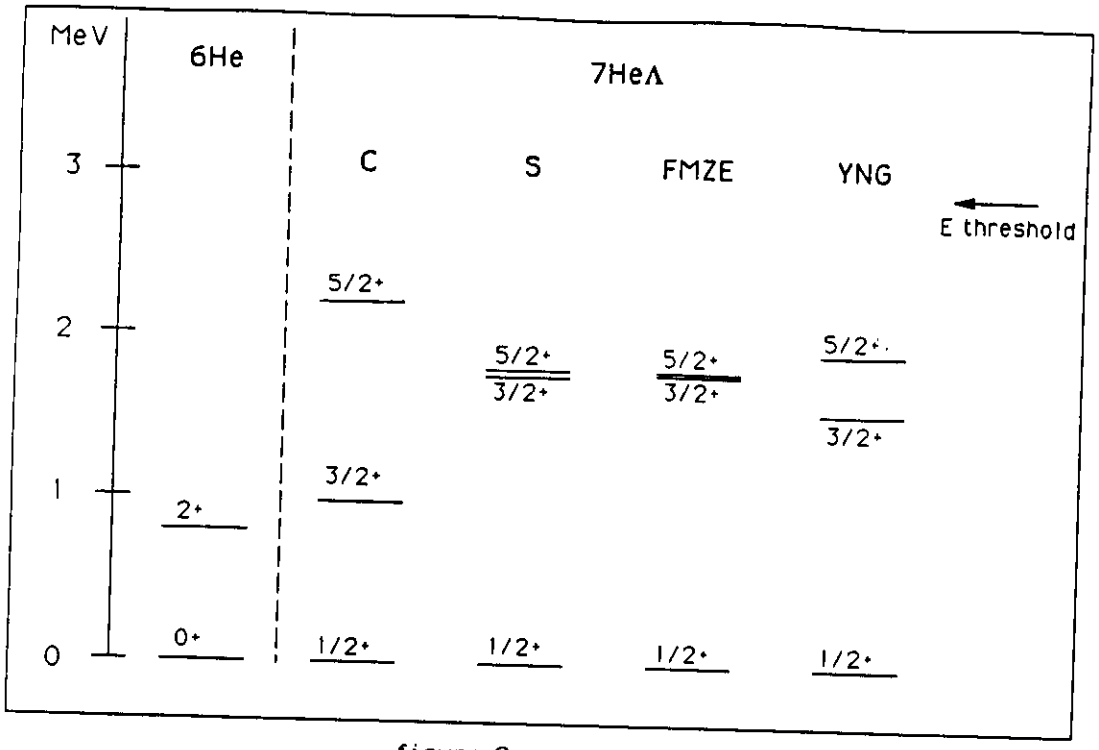

figure 2

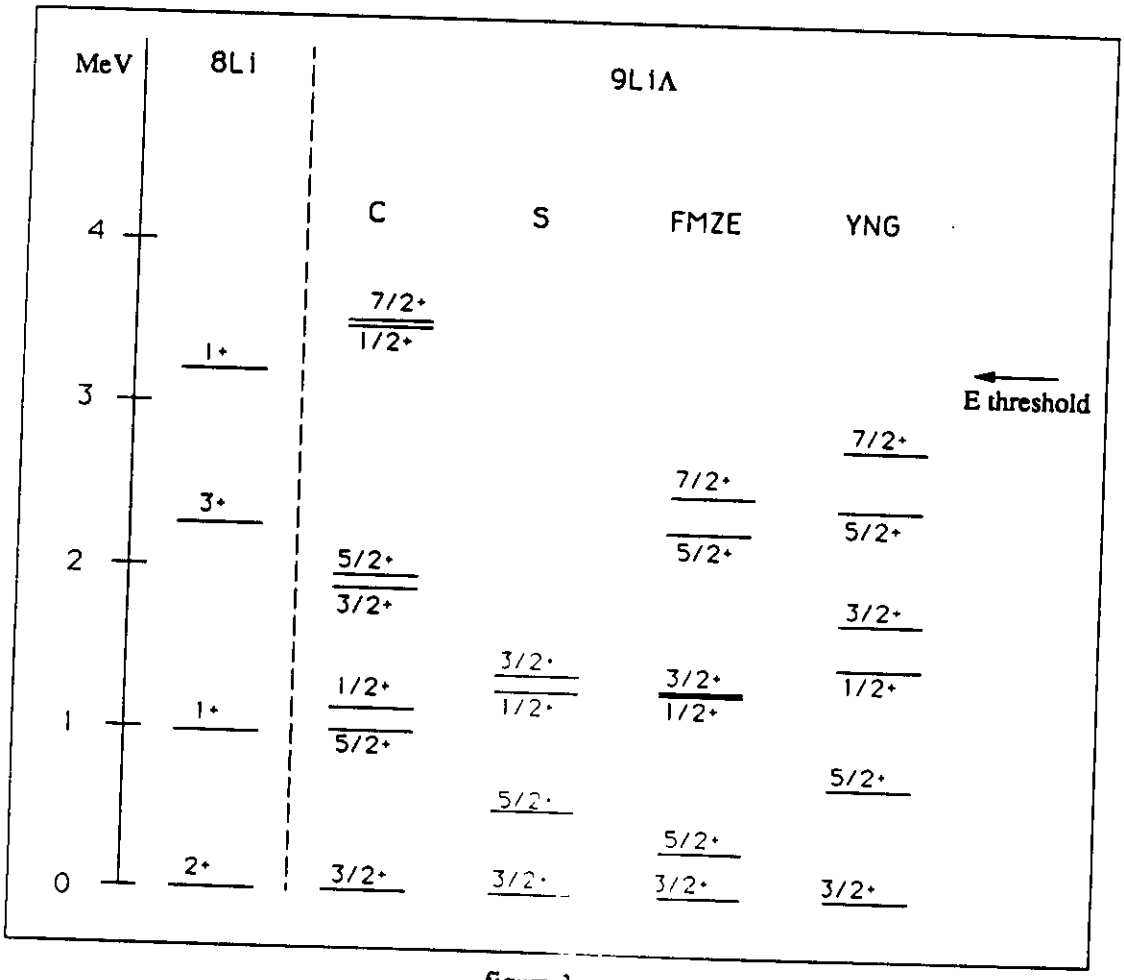

figure 3

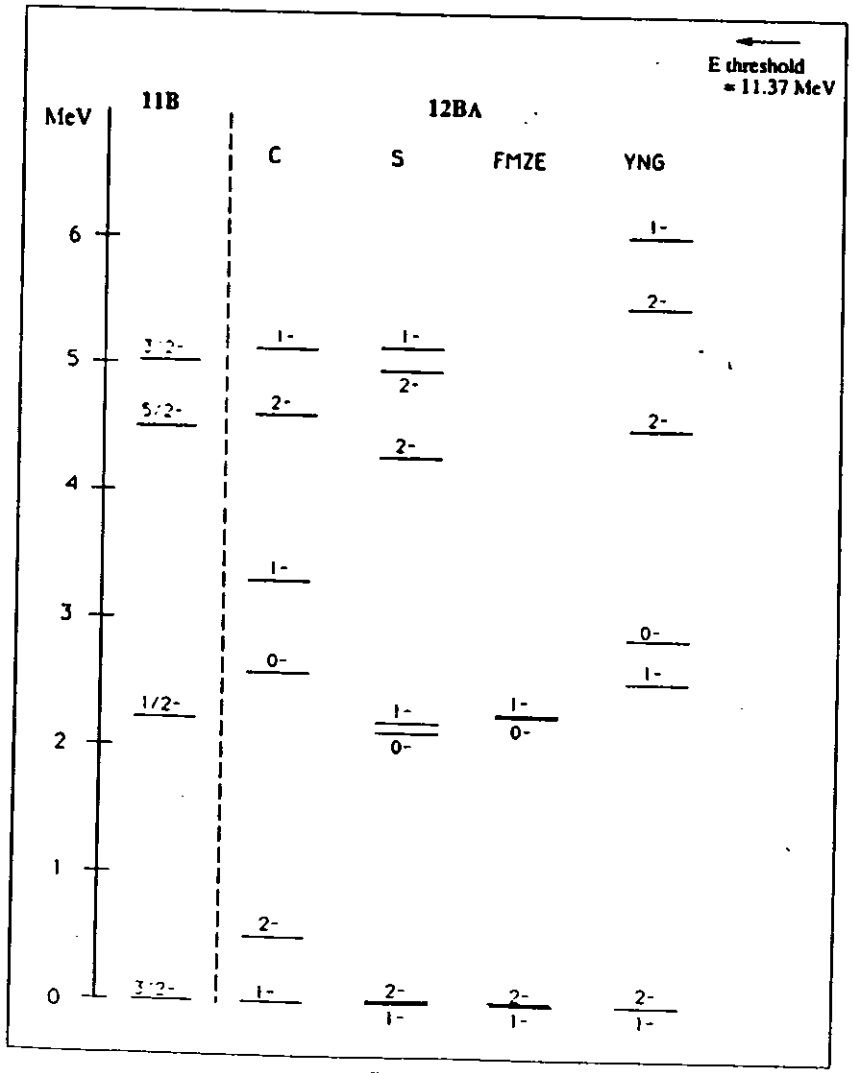

figure 4

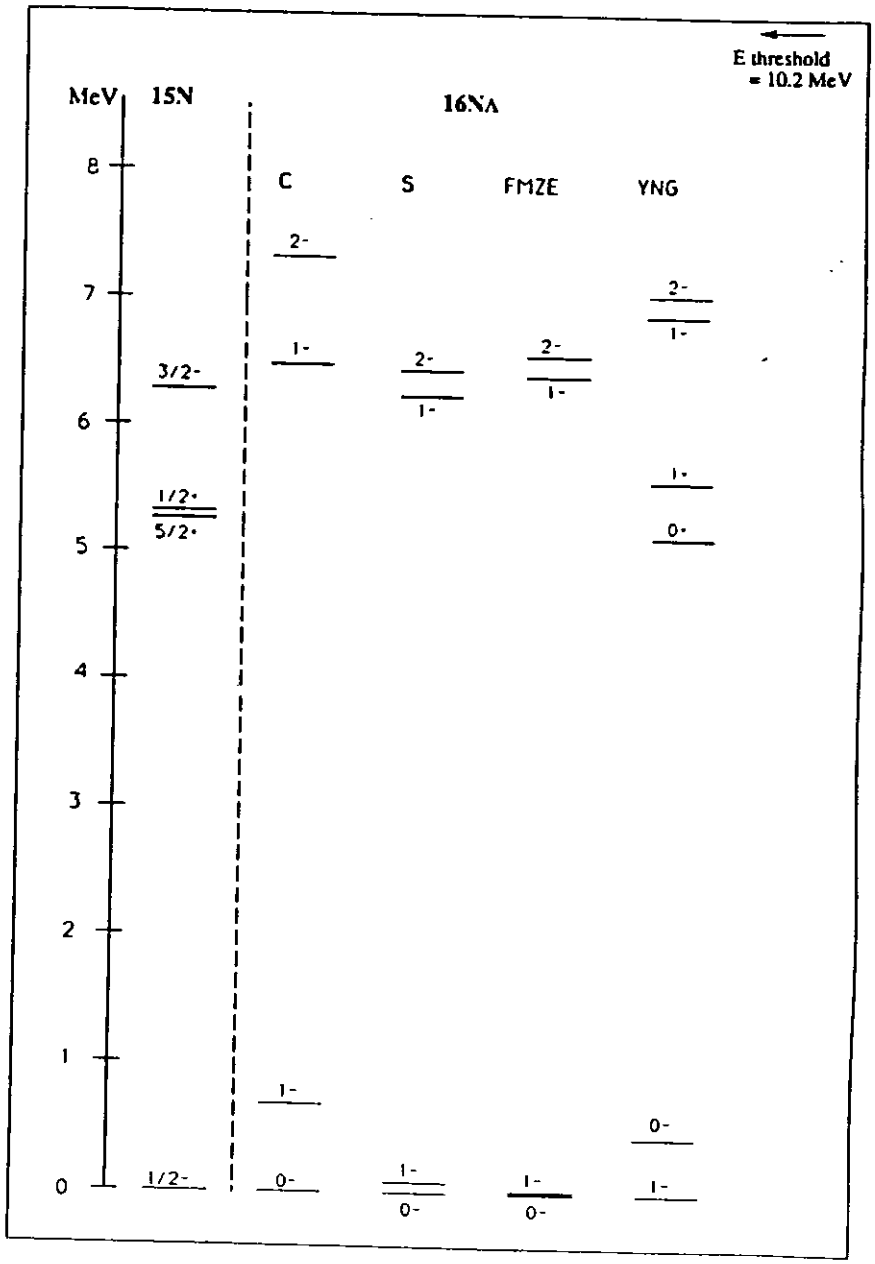

figure 5

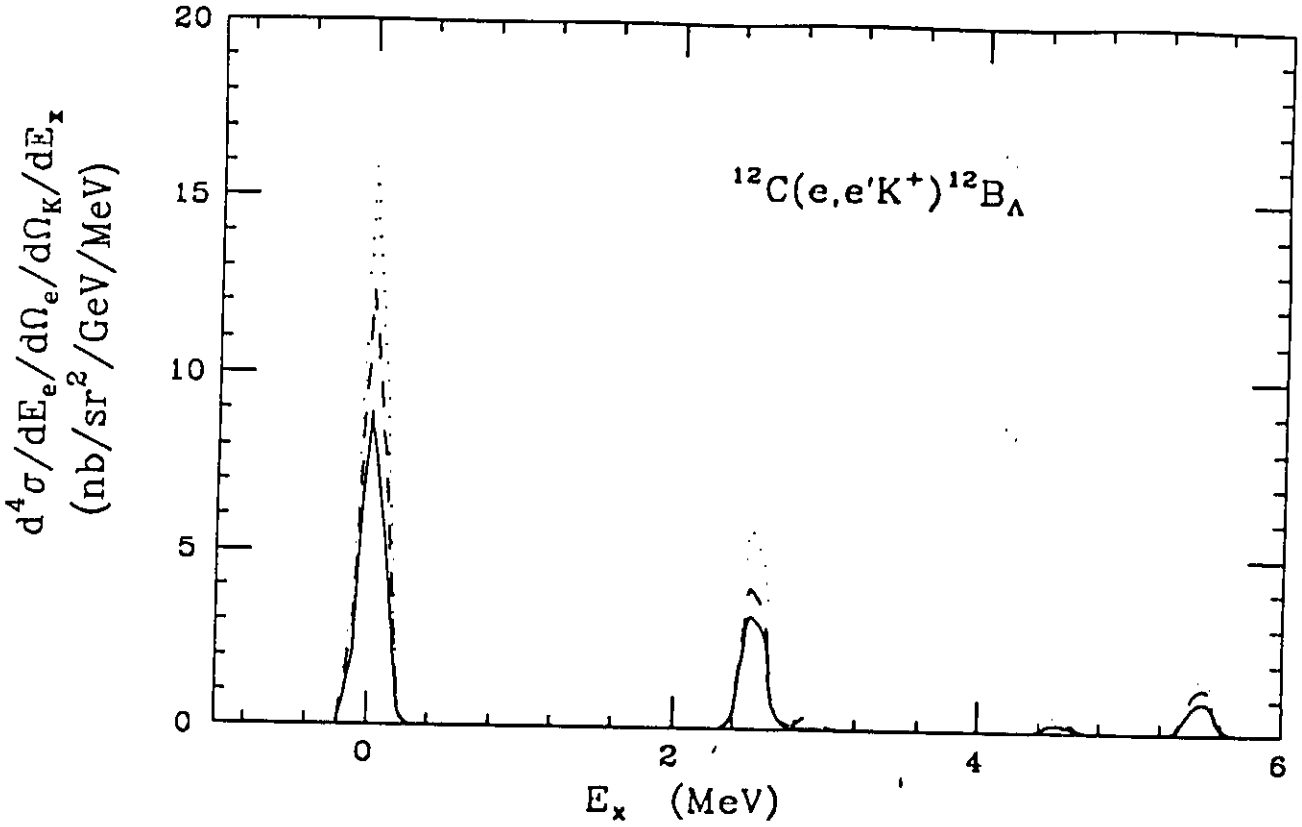
$^{12}C(e,e'K^+)^{12}B_\Lambda$
$d^4\sigma/dE_e/d\Omega_e/d\Omega_K/dE_x$ (nb/sr^2/GeV/MeV)
E_x (MeV)
0
5
10
15
20
0
2
4
6

Fig. 6

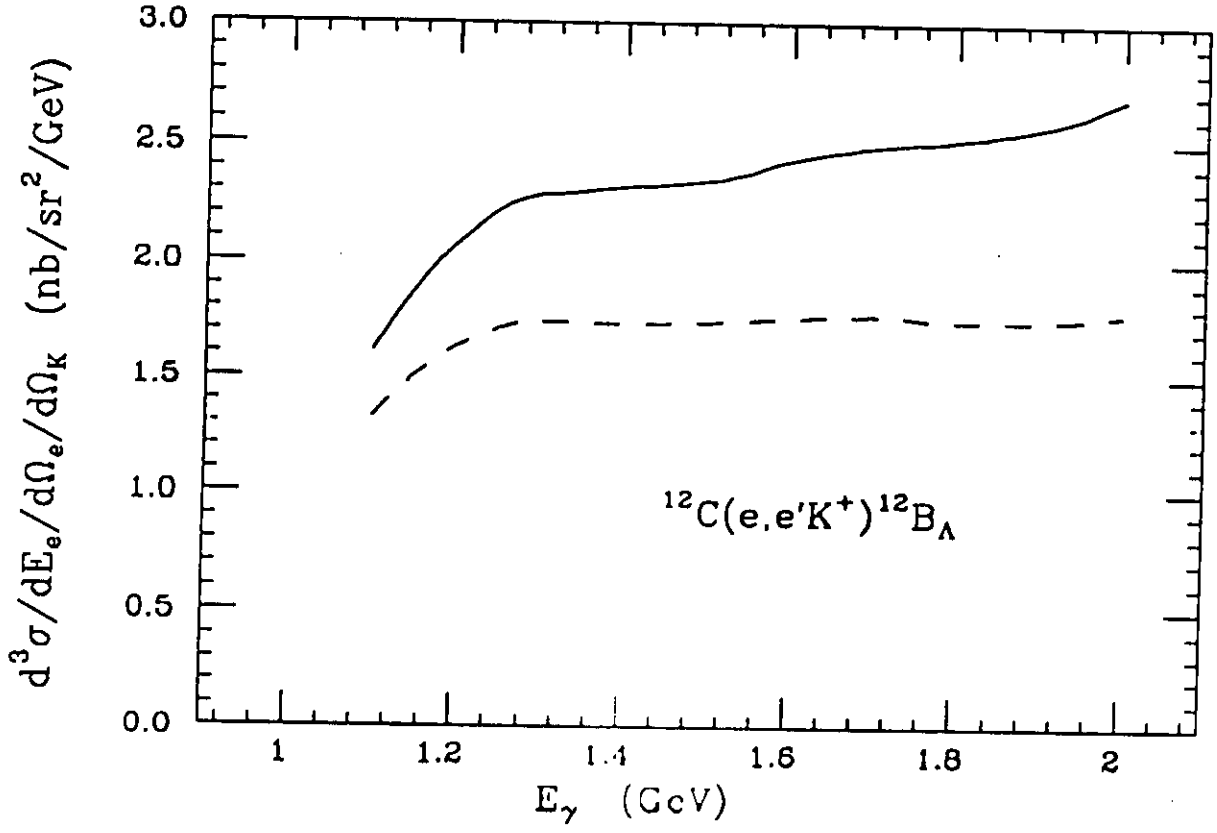
$^{12}C(e,e'K^+)^{12}B_\Lambda$
$d^3\sigma/dE_e/d\Omega_e/d\Omega_K$ (nb/sr^2/GeV)
E_γ (GeV)
0.0
0.5
1.0
1.5
2.0
2.5
3.0
1
1.2
1.4
1.6
1.8
2

Fig. 7

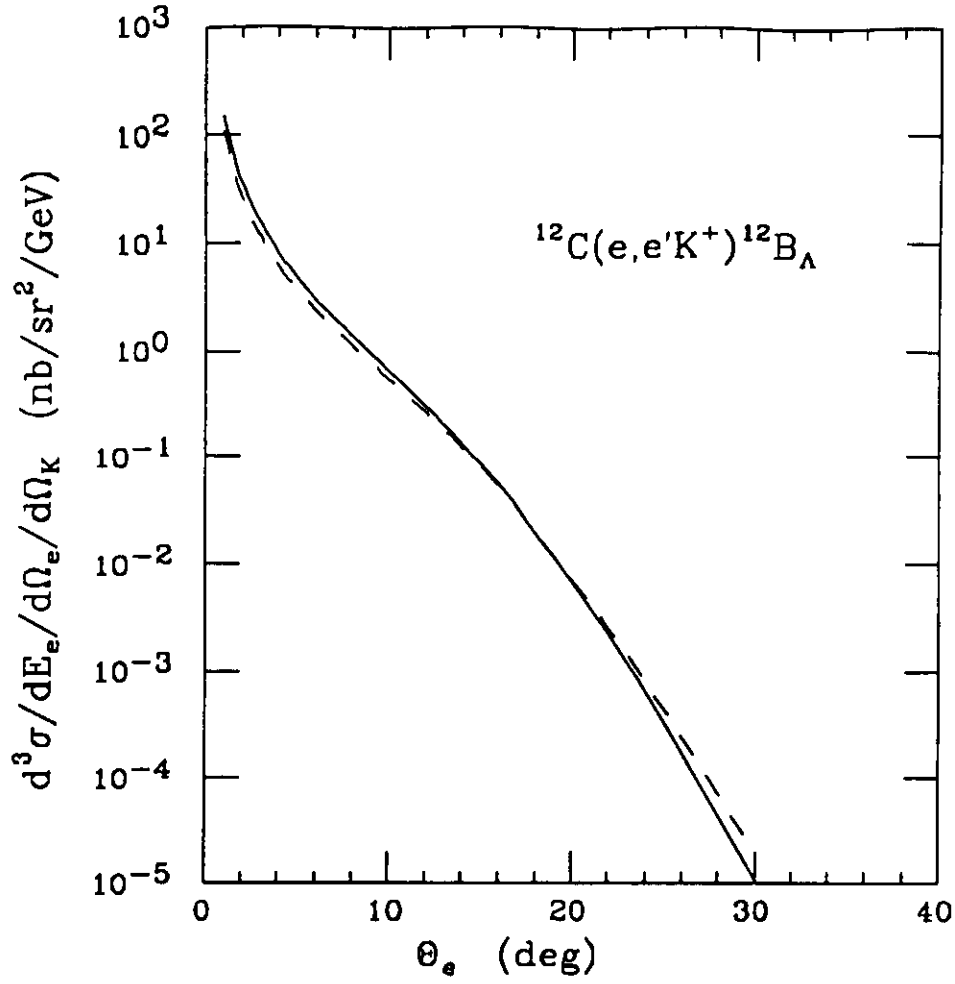
$^{12}C(e,e'K^+)^{12}B_\Lambda$
$d^3\sigma/dE_e/d\Omega_e/d\Omega_K$ (nb/sr^2/GeV)
Θ_e (deg)

Fig. 8

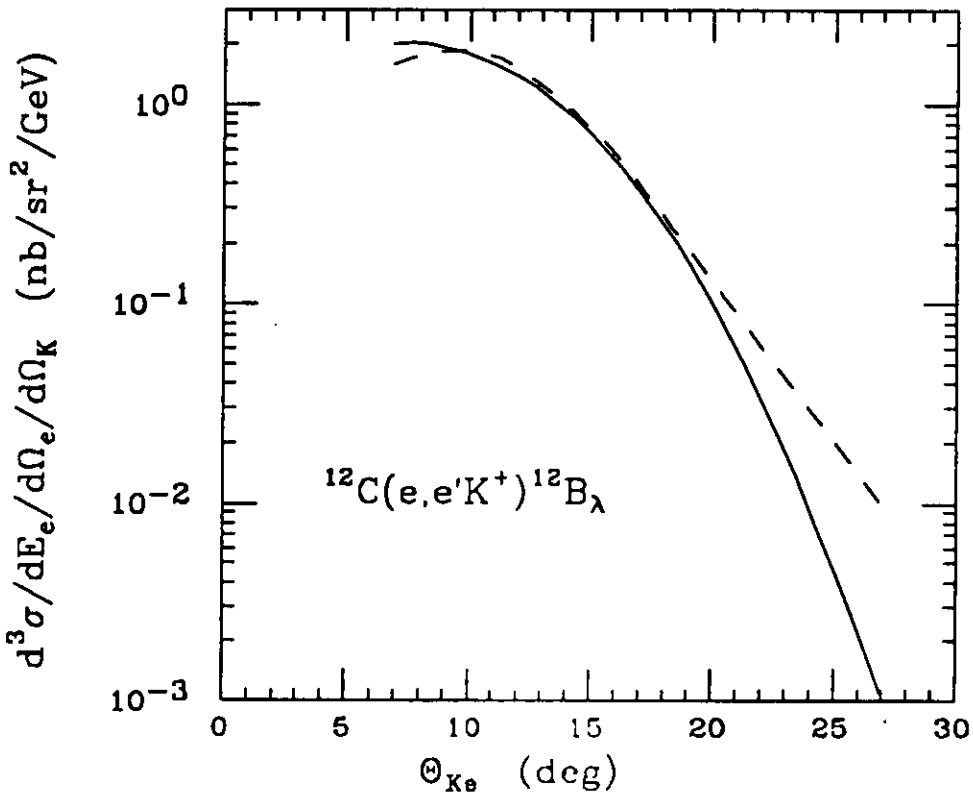
$^{12}C(e,e'K^+)^{12}B_\lambda$
$d^3\sigma/dE_e/d\Omega_e/d\Omega_K$ (nb/sr^2/GeV)
Θ_{Ke} (deg)

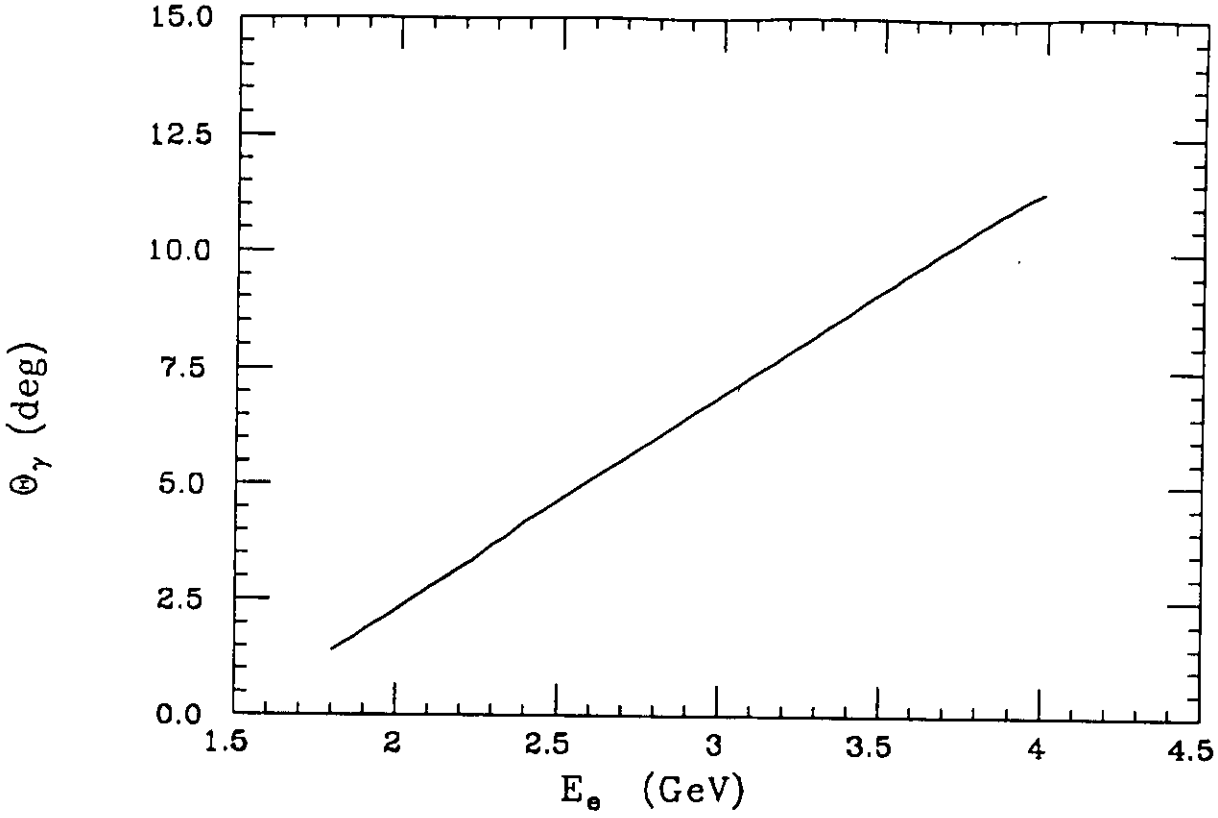
15.0
12.5
10.0
7.5
5.0
2.5
0.0
1.5
2
2.5
3
3.5
4
4.5
Θ_γ (deg)
E_e (GeV)

Fig. 10

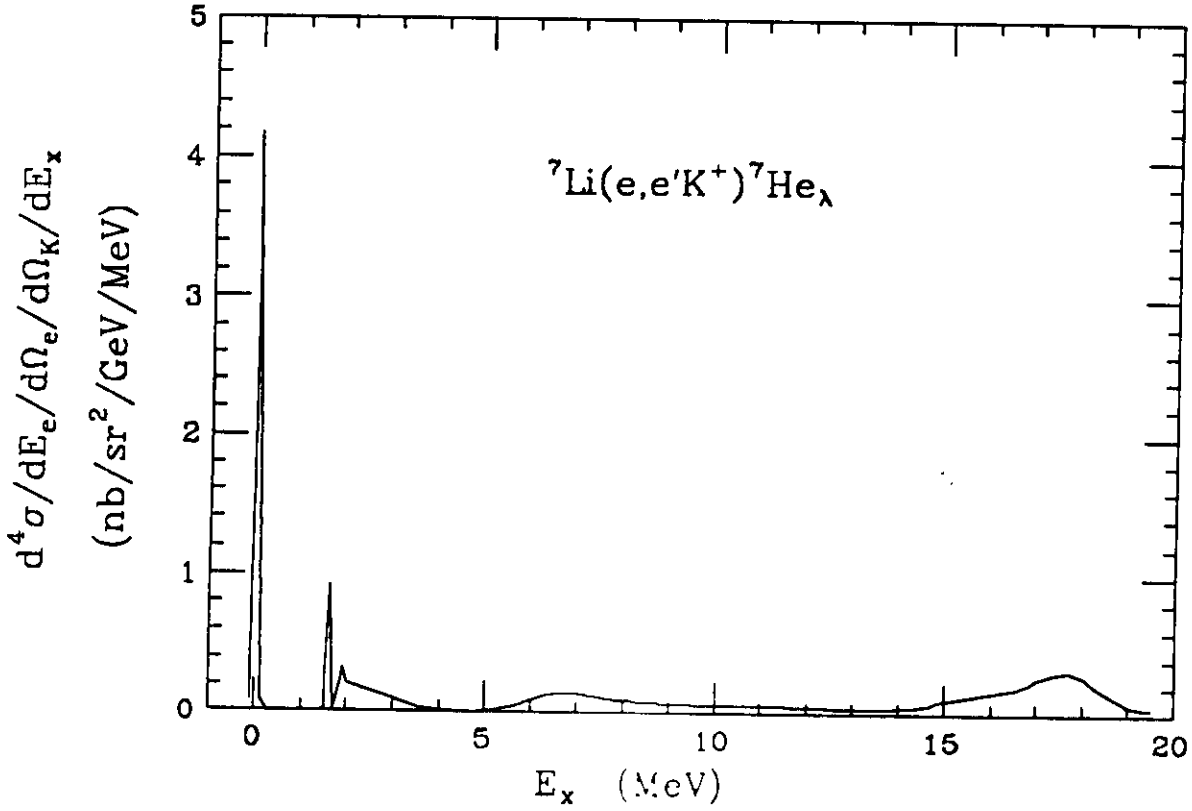
^{7}Li(e,e'K$^+$)^{7}He$_\Lambda$
5
4
3
2
1
0
0
5
10
15
20
$d^4\sigma/dE_e/d\Omega_e/d\Omega_K/dE_x$
(nb/sr^2/GeV/MeV)
E_x (MeV)

Fig. 11

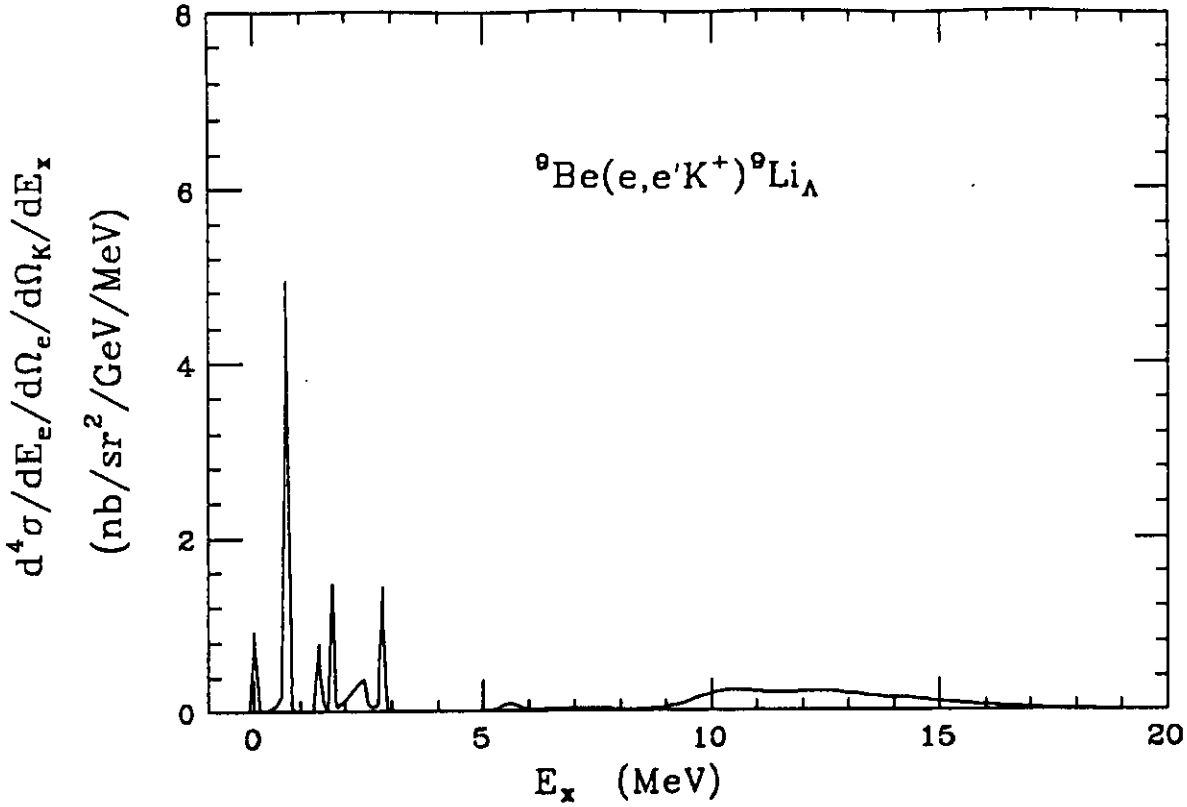
$^{9}Be(e,e'K^{+})^{9}Li_{\Lambda}$
$d^4\sigma/dE_e/d\Omega_e/d\Omega_K/dE_x$
(nb/sr^2/GeV/MeV)
E_x (MeV)
0
2
4
6
8
0
5
10
15
20

Fig. 12

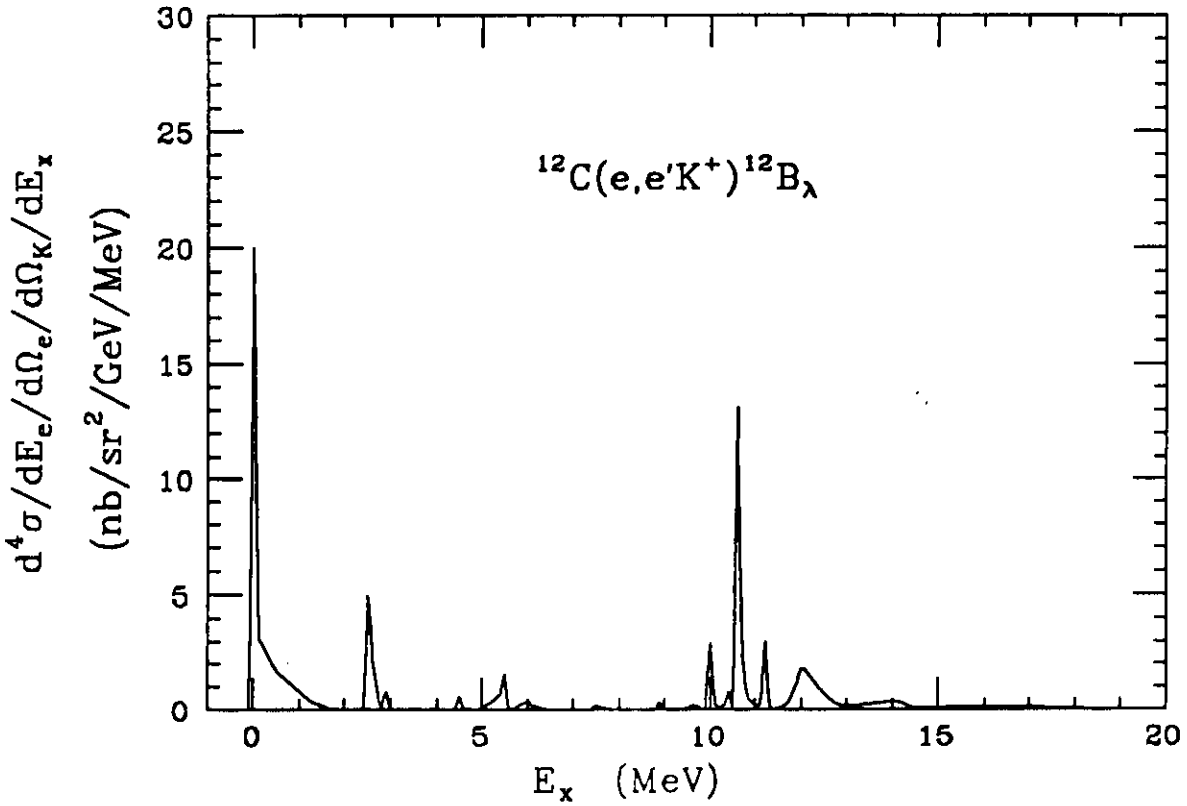
$^{12}C(e,e'K^{+})^{12}B_{\Lambda}$
$d^4\sigma/dE_e/d\Omega_e/d\Omega_K/dE_x$
(nb/sr^2/GeV/MeV)
E_x (MeV)
0
5
10
15
20
25
30
0
5
10
15
20

Fig. 13

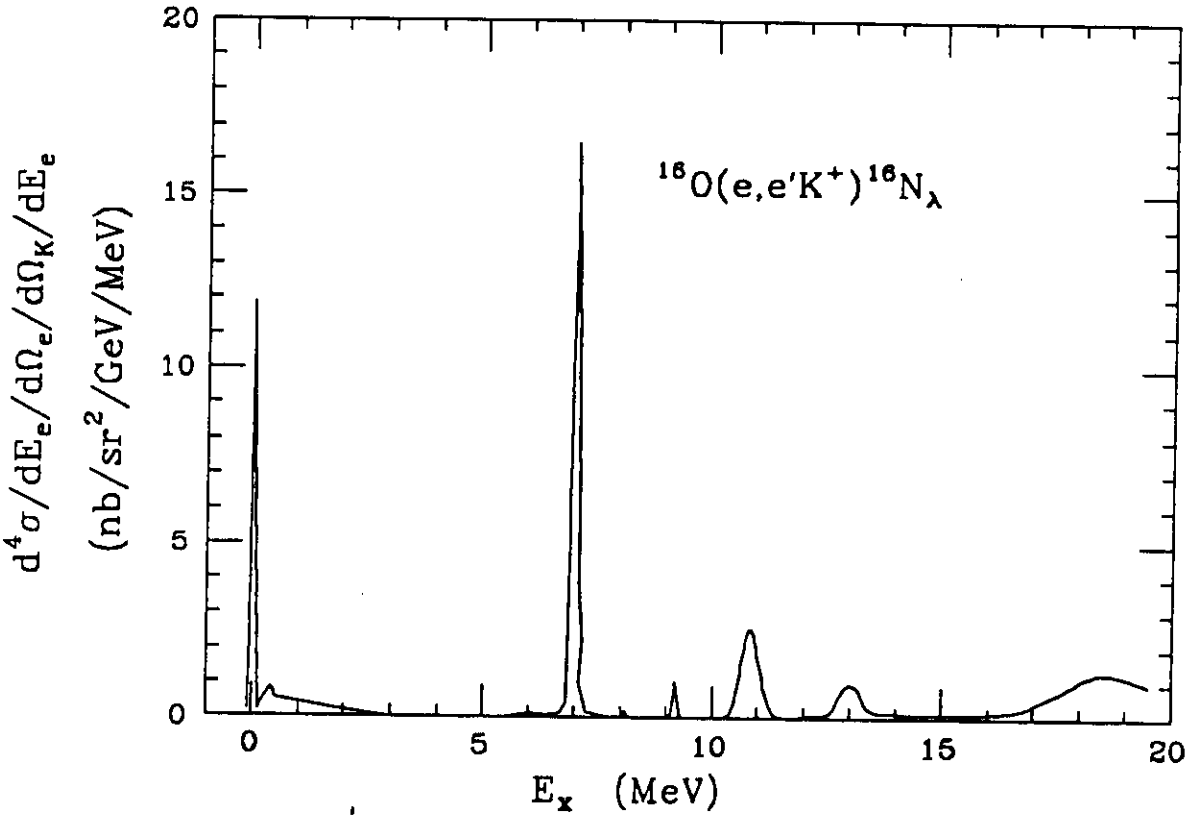
$^{16}O(e,e'K^+)^{16}N_\lambda$
$d^4\sigma/dE_e/d\Omega_e/d\Omega_K/dE_e$
(nb/sr^2/GeV/MeV)
E_x (MeV)
0
5
10
15
20

Fig. 14

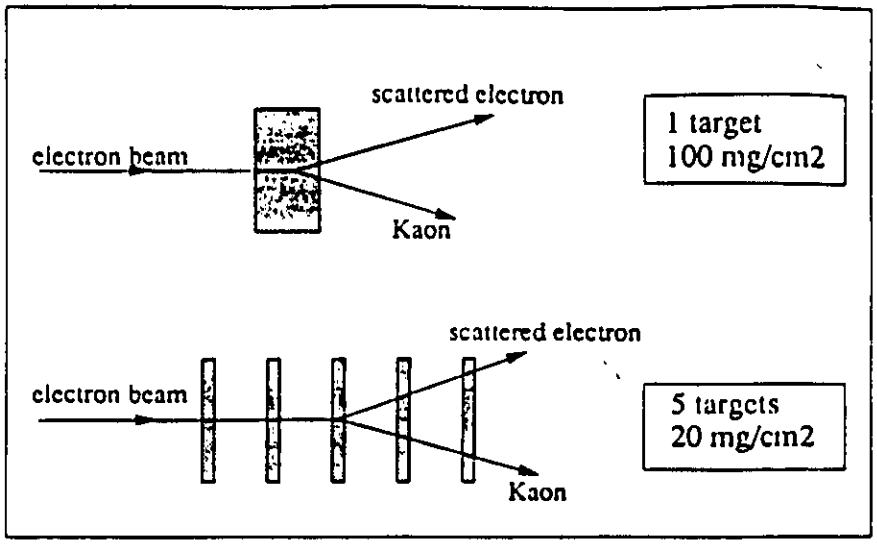

Figure 15

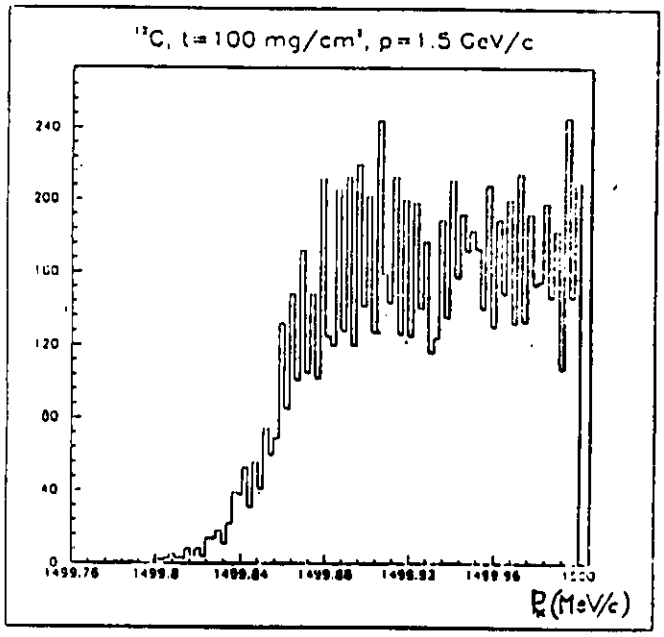

Fig. 16a

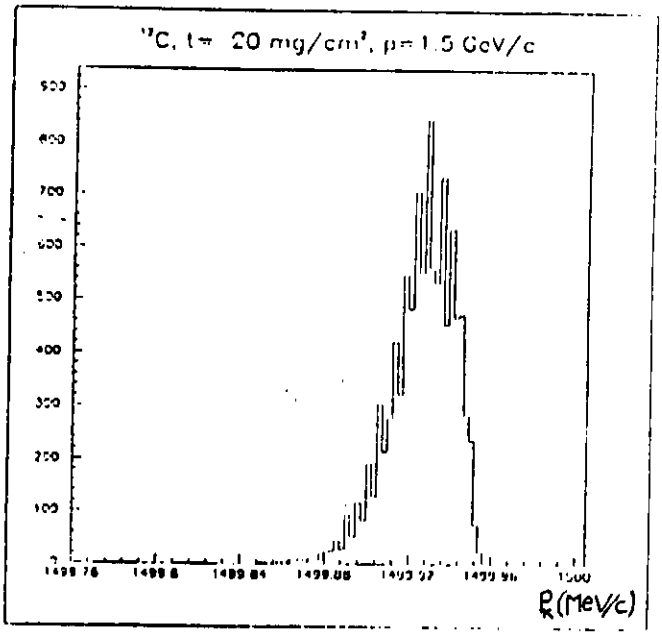

Fig. 16b